Effects of PCBM loading and thermal annealing on nanomorphology of blend of polymer/fullerene thin films solar cells: Impact on charge carrier mobility and efficiency

T. S. Shafai and O. Oklobia

Thin Films Laboratory, Faculty of Computing, Engineering, and Science, Staffordshire University, Sciences Centre, Leek Road, Stoke-on-Trent, ST4 2DF. UK.

Keywords: Photovoltaic, Thin Films, Polymer solar cell, Power conversion efficiency, electrical characterisation.

Blend of P3HT/Fullerene thin films solar cell with two different percentage ratio of PCBM loading is investigated. Optical absorption spectroscopy is employed to elucidate the nature of PCBM cluster formation upon thermal annealing. Sandwich structures comprising of ITO/Cs_2CO_3/P3HT: PCBM/LiF/Al (electron only device), and ITO/PEDOT:PSS/P3HT: PCBM/Au (hole only device) are fabricated using spin coating for the investigations concerning electron and hole mobilities. The impact of charge carrier mobilities on bimolecular recombination and ultimately the power conversion efficiency for two different PCBM loading is also investigated. A direct correlation between Langevin recombination rate and short circuit current density as a function of thermal annealing is realized. The maximum power conversion efficiency is measured at 150°C for P3HT: PCBM (1:1) solar cell.

1. Introduction

Excitonic photovoltaic devices based on polymer, Fullerene blend has been the core of many investigations [1-3]. Amongst blended material Poly Amongst blended materials, poly (3-hexylthiophene) (P3HT) and phenyl-C_{61}-butyric acid methyl ester (PCBM) are most investigated [4-5]. This is attributed to the high degree of crystallinity, reasonably high hole mobility and absorption spectrum extending in the region of 650 nm in P3HT, and suitable electronic band gap favouring efficient charge transfer. Whilst continuous improvement in power conversion efficiency employing P3HT/PCBM blend is reported [6], the breakthrough efficiency above 10% still remains unachieved. Many researchers focussed their work on either vapour or thermal annealing or combination of the processes to improve crystanility [7]. Recently we reported on the annealing strategies and its impact on charge carrier mobilitities and ultimately power conversion efficiency [8]. Effects of PCBM percentage loading on power conversion efficiency has been the subject of many reports [9-11]. It is well

established that the best power conversion efficiency results from blend with 1:1 ratio of PCBM to P3HT. Previously we reported on the effects of PCBM loading and thermal annealing on optical absorption and electrical properties of these blend [8]. The nanostructuring resulting from thermal annealing is of considerable interest as it is desired to have efficient exciton dissociation system as well as channel pass ways to the respective electrodes. Upon thermal annealing and restructuring of these percolated systems, the charge carriers' mobilities are influenced [12]. It is known that the charge carriers' mobility can be an instrumental factor in determination of bimolecular recombination, quenching the charges that otherwise can be transported to the respective electrodes and harvested. The aim of this manuscript is therefore to investigate the effect of PCBM loadings on charge carrier mobilities and its impact on bimolecular recombination and PCEs.

2. Experimental

P3HT (regioregularity of 96.6%, Ossila Ltd.), and PCBM (Solenne BV, The Netherlands) Details of the preparation of blends are discussed elsewhere [8]. Before device fabrication, ITO coated substrates (~ 10 Ω/cm^2) were first cleaned with deionised water, acetone, and isopropyl, sequentially in an ultrasonic bath for 10 minutes each. Cleaned substrates were transferred to a nitrogen-filled glove box. This was followed by spin casting at 5000 rpm, a layer (~ 40 nm) of PEDOT: PSS (Sigma Aldrich), onto the ITO coated substrate. PEDOT: PSS was filtered through a 0.45 μm filter prior to spin casting. The PEDOT: PSS film was baked for 10 minutes at ~150 °C. P3HT/PCBM blend films were spun casted onto the PEDOT: PSS layer and left to dry in the desiccators. To complete the device fabrication, an Al layer (~100 nm) was thermally deposited onto the active layer through a shadow mask, under a vacuum pressure of ~ 10^{-6} mbar. The device's active area, defined by the shadow mask is 0.14 cm^2. For obtaining ultraviolet-visible (UV-Vis) absorption, thin films of P3HT/PCBM blend was spun casted onto quartz substrates. UV-Vis absorption spectra were obtained using a Varian Cary 50 UV-Vis spectrophotometer. The current-voltage (*J-V*) curves were measured with a Keithley 2400 source meter in the dark and under AM 1.5, 100 mW/cm² illumination provided by an LOT Oriel 150-W solar simulator. The intensity of the illumination measured with a calibrated Si reference solar cell and meter (Newport and Oriel Instruments). The thicknesses of the thin films were determined using a DektakXT stylus profiler. All device characterisation were performed inside a nitrogen filled glove box.

3. Results and discussions

3.1 Optical absorption spectra

Optical absorption spectra for thin films of blend of P3HT/PCBM with approximate thickness of 150nm are investigated. The peak absorption intensity of P3HT increases upon thermal annealing as is evident in figure 1.

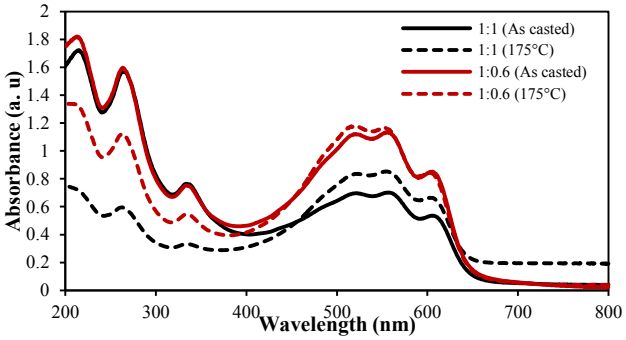

Figure 1: UV-Vis absorption spectra of P3HT: PCBM blend films, with two PCBM wt% loading (1:1 and 1:0.6); as cast and after annealing at 175°C.

This is attributed to the orderly stacking of the polymer chain back bone upon gradual increase in annealing temperature as previously reported [13]. This increase in peak absorption intensity may initiate an increase in short circuit current density. Observations of PCBM part of the spectrum reveals some interesting features. On the contrary to P3HT, the peak absorption intensity of PCBM reduces upon thermal annealing. The level of this reduction is associated with thermal annealing employed as is evident in figure 1. This is attributed to the diffusion of PCBM molecules forming needle like crystals and subsequently at higher temperatures forming clusters [14]. UV-Vis absorption spectra for blend of P3HT: PCBM with two different PCBM loading and annealed at 175 °C shown in figure 1, reveals that the peak absorption for PCBM decreases with reduced percentage loading. Furthermore upon annealing at 175 °C, the blend with highest concentration of PCBM (50% weight ratio 1:1) shows greater reduction in intensity (other annealing temperatures are not shown here). Also the peak intensities corresponding to P3HT show a small but noticeable increase and shift towards lower wavelength. In addition the vibronic shoulders appear to be more pronounced for as casted films. However at higher annealing temperatures this shoulder tends to smooth out. This is indicative of a disruption in interaction of P3HT polymer chains by PCBM molecules [15]. Whilst the peak optical absorption intensity of the PCBM has little to

do with the current density, its cluster formation i.e. size, distribution, orientations, etc., may or may not result in more efficient exciton dissociation [16].

3.2 Charge carriers mobility measurements

Figure 2, represents dark current density-voltage characteristics for electron only device comprising of sandwich structure of ITO/Cs_2CO_3/P3HT:PCBM/LiF/Al, with Cs_2CO_3 acting as the hole blocking layer. For forward bias ITO is positively biased with respect to Al. At low applied effective voltage V_{eff}, the current density voltage obeys Ohm's law and the relationship may be written as [17]

$$J = qn_{e(h)}\mu_{e(h)}\frac{V}{d} \tag{1}$$

where q is the electron charge, $\mu_{e(h)}$ is electron (hole) carrier mobility, $n_{e(h)}$ is the electron (hole) concentration, and d is the device active layer thickness. At higher effective applied field the current density voltage relationship departs from Ohmic behaviour and follows space charge limited current (SCLC). The current density dependence on voltage for trap filled limited SCLC is given by the square law [18]

$$J=\frac{9}{8}\varepsilon_0\varepsilon_r\mu_{e(h)}\frac{V^2}{d^3} \tag{2}$$

where ε_0 represents permittivity of free space, ε_r is dielectric constant of the blended material ε_r ~3.4, $\mu_{e(h)}$ is electron (hole) carrier mobility and d is the device active layer thickness ~150 nm. Using the slope corresponding to the square law in figure 2 and appropriate parameters from equation (2) yield electron mobility for as cast and annealed device for both PCBM percentage loadings.

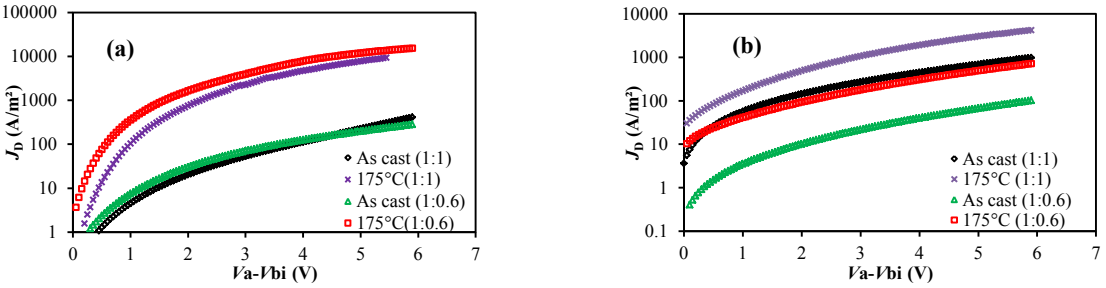

Figure 2: Dark J – V characteristics for (a) electron – only and (b) hole – only devices based on P3HT: PCBM blend of ratios, 1:1 and 1:0.6; as cast and after annealing at 175°C.

These are presented in Table 1 (a and b). Up to a thermal annealing temperature of 150 °C a continuous improvement in electron mobility is observed for both PCBM percentages loading. However above this temperature deterioration of this parameter is recorded. Similar observation for hole only device using ITO/PEDOT: PSS/P3HT: PCBM/Au sandwich structure is shown in figure 2(b). Upon positive application of voltage to Au contact with respect to PEDOT: PSS, there is no potential barrier and holes are injected from Au into HOMO of P3HT (reverse bias). As is observed for 1:1 device the hole mobility tend to remain almost constant up to a temperature of 150 °C and a sharp increase above this temperature is recorded. A similar observation for 1:0.6 devices is also realized with onset of this increase being at lower annealing temperature of 125 °C. Having calculated the charge carrier mobilities, the electron and hole density can be determined using the slope of the Ohmic region together with values of the parameters in equation 1. These are also tabulated in Table 1.

Table 1: Summary of charge carrier mobilities (μ_e: electron mobility, and μ_h: hole mobility), electron (n_e) and hole (n_h) density, bimolecular recombination constant, B_L, and recombination rate, R_L for P3HT: PCBM solar cells of ratios; (A) 1:1, and (B)1:0.6, as a function of thermal annealing.

(a)	**1:1**					
Temperature	μ_e	μ_h	n_e	n_h	B_L	R_L
As cast	1.46×10^{-9}	1.54×10^{-9}	1.30×10^{21}	3.22×10^{22}	7.77×10^{-18}	3.25×10^{26}
50°C	4.31×10^{-9}	1.33×10^{-9}	4.92×10^{21}	3.12×10^{22}	7.08×10^{-18}	1.09×10^{27}
75°C	3.06×10^{-8}	1.27×10^{-9}	4.38×10^{21}	2.70×10^{22}	6.76×10^{-18}	7.99×10^{26}
100°C	8.96×10^{-8}	1.56×10^{-9}	4.22×10^{21}	2.16×10^{22}	8.30×10^{-18}	7.57×10^{26}
125°C	5.39×10^{-8}	2.59×10^{-9}	2.82×10^{21}	1.69×10^{22}	1.37×10^{-17}	6.53×10^{26}
150°C	5.71×10^{-8}	2.57×10^{-9}	1.42×10^{21}	1.46×10^{22}	1.37×10^{-17}	2.84×10^{26}
175°C	3.98×10^{-8}	9.10×10^{-9}	7.24×10^{20}	1.66×10^{22}	4.84×10^{-17}	5.82×10^{26}
(b)	**1:0.6**					
Temperature	μ_e	μ_h	n_e	n_h	B_L	R_L
As cast	8.39×10^{-10}	4.8×10^{-10}	4.76×10^{21}	1.17×10^{22}	2.55×10^{-18}	1.42×10^{26}
50°C	1.84×10^{-9}	5.31×10^{-10}	6.55×10^{21}	1.15×10^{22}	2.82×10^{-18}	2.12×10^{26}
75°C	1.61×10^{-8}	5.00×10^{-10}	8.56×10^{21}	4.93×10^{22}	2.66×10^{-18}	1.12×10^{27}
100°C	4.38×10^{-8}	6.75×10^{-10}	2.08×10^{22}	7.52×10^{21}	3.59×10^{-18}	5.62×10^{26}
125°C	5.00×10^{-8}	1.72×10^{-9}	7.27×10^{21}	1.07×10^{22}	9.15×10^{-18}	7.12×10^{26}
150°C	3.87×10^{-8}	1.95×10^{-9}	5.29×10^{21}	1.21×10^{22}	1.04×10^{-17}	6.66×10^{26}
175°C	2.96×10^{-8}	3.19×10^{-9}	1.90×10^{21}	1.22×10^{22}	1.70×10^{-17}	3.94×10^{26}

In order to account for the exciton losses in low mobility materials, bimolecular recombination mechanism is investigated. Bimolecular recombination or Langevin recombination rate is given by [19]

$$R_L = B_L n_e . n_h \quad (3)$$

where n_e and n_h are the charge carrier density B_L is the Langevin coefficient given by [20]

$$B_L = \frac{q\mu}{\varepsilon_0 \varepsilon_r} \tag{4}$$

where q is the electronic charge, $\varepsilon_0\varepsilon_r$ is the effective dielectric constant and μ is the lower value of the electron or hole mobility [21]. Extracting data presented in table 1 and using equation 3 and 4 leads us to the bimolecular recombination rates. As is evident for 1:1 device the recombination rate decreases with increasing annealing temperature up to a temperature of 150 °C, indicating the bimolecular recombination may not play a dominant role as compared to the trap assisted model (Shockley- Reed- Hall) as we have previously reported. However for 1:0.6 devices, no correlation between thermal annealing and recombination rate is observed unlike 1:1 devices.

3.3 Power Conversion Efficiency

Figure 3 shows current density-voltage characteristics for as cast and annealed device for two different PCBM loading.

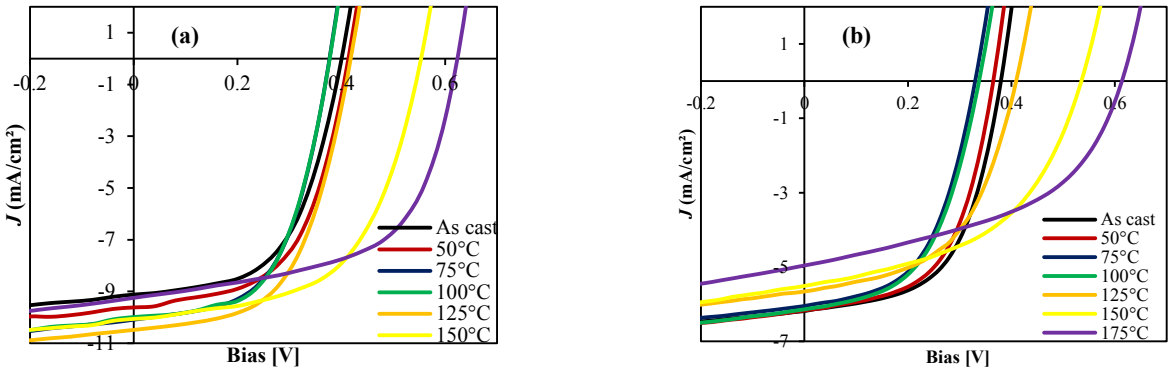

Figure 4: *J-V* curves under illumination for devices based on P3HT:PCBM: (a) 1:1, and (b) 1:0.6; as a function of thermal annealing.

As can be observed the maximum short circuit current density corresponds to at temperature of 150 °C (1:1 device). This correlates well with the lowest recombination rates recorded at this temperature. It should be pointed out that the maximum exciton generation rate has also been deduced at this temperature as we have previously reported [16]. However for 1:0.6 devices, no correlation between the recombination rate and the short circuit current density is observed. The Maximum open circuit voltage is measured at 175 °C this is attributed to the disruption of shunt passes and increasing space charge and lowering charge extraction as is evident in the reduction in electron density for both PCBM loadings in Table 1. The power

conversion efficiencies tend to follow the same trend as the short circuit current density, with the highest PCE recorded at 150 °C for 1:1 device.

4. Conclusions

A percolated system consisting of PCBM/P3HT with different percentage weigh ratio showing nanostructuring and is responsive to thermal annealing is investigated. We have quantitatively examined the optical absorption and optical images obtained from thin film devices and established that cluster formation enlarges upon thermal annealing. Furthermore we established that the optical absorption intensity for PCBM part of the spectrum reduces with annealing temperatures and the absorption intensity reduction is highest for devices with largest PCBM percentage weight ratio. Measurements for charge carriers' mobility with annealing temperature proved instrumental in establishing the dependence of bimolecular recombination rate on thermal annealing. Whilst a direct correlation between bimolecular recombination and short circuit current density is observed for 1:1 device, we were unable to establish the same trend for 1:0.6 percentage weight ratios. The maximum power conversion efficiency is also measured for both PCBM loadings as a function of thermal annealing indicating 150 °C is the upper limit for best device efficiency.

References

[1] S. R. Forrest, M. E. Thompson, Chem. Rev. Vol. 107 (2007), p. 923-925.

[2] G. Dennler, M. C. Scharber, C. J. Brabec, Advanced Materials Vol. 21 (2009), p. 1323-1338

[3] J. Nelson, Materials Today Vol. 14 (2011), p. 462-470

[4] M. Campoy-Quiles, T. Ferenczi, T. Agostinelli, P. G. Etchegoin, Y. Kim, T. D. Anthopoulos, P. N. Stavrinou, D. D. C. Bradley, J. Nelson, Nature Materrials Vol. 7 (2008), p. 158-164

[5] F-C. Chen, C-J. Ko, J-L. Wu, W-C. Chen, Solar Energy Materials and Solar Cells, Vol. 94 (2010), p. 2426-2430

[6] G. Li, R. Zhu, Y. Yang, Nature Photonics, Vol. 6 (2012), p. 153-160

[7] H. Hoppe, N. S. Sariciftci, Journal of Materials Chemistry, Vol. 16 (2006), p. 45-61

[8] O. Oklobia, T. S. Shafai, Solid-State Electronics, Vol. 87 (2013), p. 64-68

[9] E. A. Parlak, Solar Energy Materials and Solar Cells, Vol. 100 (2012), p. 174-184

[10] D. Chirvase, J. Parisi, J. C. Hummelen, D. Dyakonov, Nanotechnology, Vol. 15 (2004), p. 1317-1323

[11] Y. Kim, S. A. Choulis, J. Nelson, D. D. C. Bradley, S. Cook, J. R. Durrant, Journal of Materials Science, Vol. 40 (2005), p. 1371-1376

[12] V. D Mihailetchi, H. Xie, D. de Boer, L. J. A. Koster, P. W. M. Blom, Advanced Functional Materials, Vol. 16 (2006), p. 699-708

[13] Y. Kim, S. A. Choulis, J. Nelson, D. D. C. Bradley, Applied Physics Letters, Vol. 86 (2005), 063502, p. 1-3

[14] A. Swinnen, I. Haeldermans, M. vande Ven, J. D'Haen, G. Vanhoyland, S. Aresu, M. D'Olieslaeger, J. Manca, Advanced Functional Materials, Vol. 16 (2005), p. 760-765

[15] Y.-C. Huang, Y.-C. Liao, S.-S. Li, M.-C. Wu, C.-W. Chen, W.-F. Su, Solar Energy Materials and Solar Cells Vol. 93 (2009), p. 888-892

[16] O. Oklobia, T. S. Shafai, Solar Energy Materials and Solar Cells, Vol. 117 (2013), p. 1-8

[17] M. A. Lampert, P. Mark: *Current Injection in Solids*, (Academic Publications, New York 1970)

[18] S. M. Sze, *Semiconductor Devices Physics and Technology*, (John Wiley & Sons Publications, Canada 1985)

[19] M. Kuik, L. J. A. Koster, G. A. H. Wetzelaer, P. W. M. Blom, Physical Review Letters, Vol. 107 (2011), p. 1-5

[20] P. Langevin, Ann. Chim. Phys. Vol. 28 (1903), p. 433

[21] L. J. A. Koster, V. D Mihailetchi, P. W. M. Blom, Applied Physics Letters, Vol. 88 (2006) 052104, p. 1-3